

# Unified Representation of Molecules and Crystals for Machine Learning

Haoyan Huo

*School of Physics, Peking University, Beijing, China*

*Present address: Department of Materials Science and Engineering, University of California, Berkeley, USA*

Matthias Rupp

*Fritz Haber Institute of the Max Planck Society, Berlin, Germany*

*Department of Computer and Information Science, University of Konstanz, Germany*

*Present address: Materials Research and Technology Department,*

*Luxembourg Institute of Science and Technology (LIST), Belvaux, Luxembourg\**

(Dated: November 28, 2022)

Accurate simulations of atomistic systems from first principles are limited by computational cost. In high-throughput settings, machine learning can reduce these costs significantly by accurately interpolating between reference calculations. For this, kernel learning approaches crucially require a representation that accommodates arbitrary atomistic systems. We introduce a many-body tensor representation that is invariant to translations, rotations, and nuclear permutations of same elements, unique, differentiable, can represent molecules and crystals, and is fast to compute. Empirical evidence for competitive energy and force prediction errors is presented for changes in molecular structure, crystal chemistry, and molecular dynamics using kernel regression and symmetric gradient-domain machine learning as models. Applicability is demonstrated for phase diagrams of Pt-group/transition-metal binary systems.

This study has been published. See DOI 10.1088/2632-2153/aca005 for the version of record.

## INTRODUCTION

The computational study of atomistic systems such as molecules and crystals requires accurate treatment of interactions at the atomic and electronic scale. Accurate first-principles methods, however, are limited by their high computational cost. In settings that require many calculations, such as dynamics simulations, phase diagrams, or high-throughput searches, machine learning (ML) [1,2] can reduce overall costs by orders of magnitude via accurate interpolation between reference calculations. [3–5] For this, the problem of repeatedly solving a complex equation such as Schrödinger’s equation *for many related inputs* is mapped onto a non-linear regression problem: Instead of numerically solving new systems, they are statistically estimated based on a reference set of known solutions. [6,7] This ansatz enables, among other applications, screening larger databases of molecules and materials [5,8], running longer dynamics simulations [9], investigating larger systems [10], and increasing the accuracy of calculations [5,11].

Kernel-based ML models [12–15] for data-efficient accurate prediction of ab initio properties require a single space in which regression is carried out. Representations [16] are functions that map atomistic systems to elements in such spaces, either directly or via a kernel [17]. Representations should be (i) *invariant* against transformations preserving the predicted property, in particular translations, rotations, and nuclear permutations of same elements, as learning these invariances from data would require many reference calculations; non-scalar properties can require equivariance instead of invariance; (ii) *unique*, that is, variant against transformations changing the property, as systems with identical representation that differ in property would introduce errors [18]; (iii) *continuous*, and ideally *differentiable*, as discontinuities work against the smoothness assumption of the ML model and model gradients are often useful; (iv) *general* in the sense of being able to en-

code any atomistic system, including finite and periodic systems; (v) *fast* to compute, as the goal is to reduce computational cost; (vi) *data-efficient* in the sense of requiring few reference calculations to reach a given target error. Constant size is an advantage, [19] as is the ability to encode the whole system as well as local atomic environments. Requirements (v) and (vi) are in practice determined empirically. See Refs. 16,20–22 for details on these and further requirements.

Some representations fulfill these requirements only partially, such as the Coulomb matrix (CM) [6] and bag of bonds (BoB) [23] discussed below. State-of-the-art representations often fulfill these requirements in some limit, such as infinite expansion order. See Ref. 16 for a comprehensive and detailed discussion. The descriptors used in cheminformatics, [24] and sometimes in materials informatics, often violate (ii) and (iii), in particular if they do not include atomic coordinate information or rely on cutoff-based definitions of chemical bonds. Such descriptors serve the different purpose of predicting derived properties that are not functions of a single conformation, such as solubility or binding affinity to a macromolecule.

We introduce a many-body tensor representation (MBTR) derived from CM/BoB and concepts of many-body expansions. It is related [16] to Behler-Parrinello symmetry functions [25] and histograms of distances, angles, and dihedral angles [26]. MBTR fulfills the above requirements in the limit, is interpretable, allows visualization (Figure 1), and describes finite and periodic systems. State-of-the-art empirical performance is demonstrated by us for organic molecules and inorganic crystals, as well as applicability to phase diagrams of Pt-group/transition metal binary systems, and by others for predicting and optimizing various molecular [27–33] and crystalline properties [34–37]. Implementations of MBTR are publicly available (see Code Availability section at the end).

## METHOD

We start from the CM [6, 10, 38], which represents a molecule  $\mathcal{M}$  as a symmetric atom-by-atom matrix

$$\mathbf{M}_{i,j} = \begin{cases} \frac{1}{2} Z_i^{2.4} & i = j \\ \frac{Z_i Z_j}{d_{i,j}} & i \neq j \end{cases}, \quad (1)$$

where  $Z_i$  are atomic numbers and  $d_{i,j} = \|\mathbf{R}_i - \mathbf{R}_j\|$  is Euclidean distance between atoms  $i$  and  $j$ . To avoid dependence on atom ordering (in the input), which would violate (i),  $\mathbf{M}$  is either diagonalized, losing information which violates (ii) [18], or sorted, causing discontinuities that violate (iii). Another shortcoming is the use of  $Z$ , which is not well suited for interpolation [39] as it overly decorrelates chemical elements from the same column of the periodic table.

The related BoB [23] representation uses the same terms, but arranges them differently. For each pair of chemical elements, corresponding CM terms are stored in sorted order, which can be viewed as an  $N_e \times N_e \times d$  tensor, or an  $N_e \times (N_e + 1)/2 \times d$  tensor if symmetry is taken into account, where  $N_e$  is number of elements and  $d$  is sufficiently large. Unlike the CM, it can not distinguish homometric molecules [21], which might distort its feature space [40]. While the BoB tensor itself does not suffer from discontinuities, its derivative does.

To derive MBTR, we retain stratification by elements, but avoid the sorting by arranging distances on a real-space axis:

$$f_{\text{BoB}}(x, z_1, z_2) = \sum_{i,j=1}^{N_a} \delta(x - d_{i,j}^{-1}) \delta(z_1, Z_i) \delta(z_2, Z_j), \quad (2)$$

where  $x$  is a real number,  $z_1, z_2$  are atomic numbers,  $N_a$  is number of atoms,  $\delta(\cdot)$  is Dirac’s delta, and  $\delta(\cdot, \cdot)$  is Kronecker’s delta.  $f_{\text{BoB}}$  has mixed continuous-discrete domain and encodes all (inverse) distances between atoms with elements  $z_1$  and  $z_2$ . For a smoother measure, we replace Dirac’s  $\delta$  with another probability distribution  $\mathcal{D}$ , “broadening” or “smearing” it. [20, 41] In this work, we use the normal distribution. Other distributions can be used, in particular symmetric and short-tailed ones, for example, the Laplace distribution or the uniform distribution. We did not observe significant differences in performance, however. Adding a weighting function  $w_2$  and replacing the Kronecker  $\delta$  functions by an element correlation matrix  $C \in \mathbf{R}^{N_e \times N_e}$  yields

$$f_2(x, z_1, z_2) = \sum_{i,j=1}^{N_a} w_2(i, j) \mathcal{D}(x, g_2(i, j)) C_{z_1, Z_i} C_{z_2, Z_j} \quad (3)$$

of which (2) is a special case. In general,  $g_2$  describes a relation between atoms  $i$  and  $j$ , such as their inverse distance,  $\mathcal{D}$  broadens the result of  $g_2$ , and  $w_2$  allows to weight down contributions, for example, from far-away atoms. Building on the idea of many-body expansions, [42, 43] we generalize from  $f_2$  in (3), which encodes two-body terms, to the MBTR equation

$$f_k(x, \mathbf{z}) = \sum_{i=1}^{N_a} w_k(\mathbf{i}) \mathcal{D}(x, g_k(\mathbf{i})) \prod_{j=1}^k C_{z_j, Z_{i_j}}, \quad (4)$$

where  $\mathbf{z} \in \mathbf{N}^k$  are atomic numbers,  $\mathbf{i} = (i_1, \dots, i_k) \in \{1, \dots, N_a\}^k$  are index tuples, and  $w_k, g_k$  assign a scalar to  $k$  atoms in  $\mathcal{M}$ . [44] Canonical choices of  $g_k$  for  $k = 1, 2, 3, 4$  are atom counts, (inverse) distances, angles, and dihedral angles. The element correlation matrices  $C$  allow exploitation of similarities between chemical element species (“alchemical learning”), for example, within the same column of the periodic table. [45–47]

We measure the similarity of two atomistic systems  $\mathcal{M}$  and  $\mathcal{M}'$  as the Euclidean distance between their representations,

$$d_k^2(\mathcal{M}, \mathcal{M}') = \sum_{\mathbf{z}} \int (f_k(x, \mathbf{z}) - f'_k(x, \mathbf{z}))^2 dx. \quad (5)$$

In practice, we adjust (4) for symmetries. Discretizing the continuous axis as  $(x_{\min}, x_{\min} + \Delta x, \dots, x_{\max})$  results in a rank  $k+1$  tensor of dimensions  $N_e \times \dots \times N_e \times N_x$  with  $N_x = (x_{\max} - x_{\min})/\Delta x$ , where  $x_{\min}$  and  $x_{\max}$  are the smallest and largest values for which  $f_k(x, \mathbf{z}) \neq 0$  for all  $\mathbf{z}$  and  $\mathcal{M}$ . Linearizing element ranks yields  $N_e^k \times N_x$  matrices, allowing for visualization (Figure 1) and efficient numerical implementation via linear algebra routines. For systems with many element species, discretization can lead to large matrices, requiring substantial amounts of memory. In such settings, memory-efficient implementation via sparse matrix formats or on-the-fly calculation of distances and inner products (see, e.g., Ref. 45) of MBTR matrices might be preferable.

Periodic systems, used to model bulk crystals and surfaces, can be viewed as unit cells surrounded by infinitely many translated images of themselves. For such systems,  $N_a = \infty$  and the sum in (4) diverges. We prevent this by requiring one index of  $\mathbf{i}$  to be in the (same) primitive unit cell. [48] This accounts for translational symmetry and prevents double-counting. Use of weighting functions  $w_k$  such as exponentially decaying weights [49] then ensures convergence of the sum. Figure 1 (right) presents the resulting distribution of angles for face-centered cubic (fcc) NaCl as an example. Note that the  $k$ -body terms  $g_k$  do not depend on choice of unit cell geometry (lattice vectors). This ensures unique representation of Bravais lattices where the choice of basis vectors is not unique, for example 2D hexagonal lattices where the angle between lattice vectors can be  $\frac{1}{3}\pi$  or  $\frac{2}{3}\pi$ .

Many applications, including dynamics simulations and structural relaxation, require forces, the negative gradient of the energy with respect to atomic coordinates. The gradient of (4) is given by

$$\nabla f_k(x, \mathbf{z}) = \sum_{i=1}^{N_a} \left( \mathcal{D}(x, g_k(\mathbf{i})) \nabla w_k(\mathbf{i}) + w_k(\mathbf{i}) \frac{\partial \mathcal{D}(x, g_k)}{\partial g_k} \nabla g_k(\mathbf{i}) \right) \prod_{j=1}^k C_{z_j, Z_{i_j}}. \quad (6)$$

The gradient  $\nabla f_k(x, \mathbf{z})$  can be derived analytically if this is possible for  $\nabla w_k$ ,  $\nabla g_k$ , and  $\nabla \mathcal{D}$ . Alternatively, automatic differentiation [50, 51] can be used, removing the need for manual derivation. Figure 1 visualizes MBTR gradients.

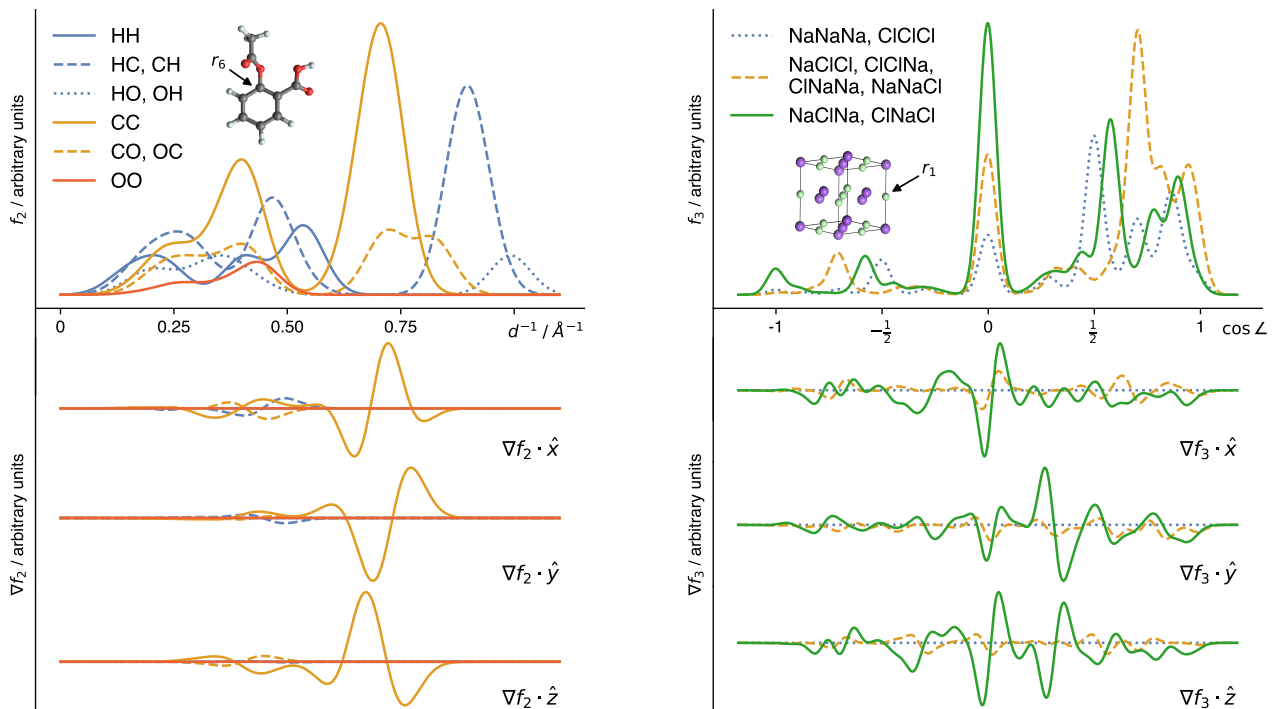


FIG. 1: *Visualization of many-body tensor representation.* Top panels show distributions of inverse distances ( $k = 2$ , quadratic weighting) for aspirin ( $\text{C}_9\text{O}_4\text{H}_8$ , left) and distributions of angles ( $k = 3$ , exponential weighting) for fcc salt (NaCl, right). Bottom panels show derivatives of the representation, obtained by differentiating with respect to the Cartesian coordinates of C atom  $r_6$  connecting the ester group (left) and the Na atom  $r_1$  at lattice point (right).

## RESULTS

To validate MBTR, we demonstrate accurate predictions for properties of molecules and crystals. Focusing on the representation, we employ plain kernel ridge regression models [7] unless stated otherwise.

### Changes in molecular structure

To demonstrate interpolation across changes in the chemical structure of molecules we utilize a benchmark dataset [38] of 7,211 small organic molecules composed of up to seven C, N, O, S and Cl atoms, saturated with H. Molecules were relaxed to their ground state using the Perdew-Burke-Ernzerhof (PBE) [52] approximation to Kohn-Sham density functional theory (DFT). Restriction to relaxed structures projects out spatial variability and allows focusing on changes in chemical structure. Table I presents prediction errors for atomization energies and isotropic polarizabilities obtained from single point calculations with the hybrid PBE0 [53, 54] functional. For 5 k training samples, prediction errors are below 1 kcal/mol (“chemical accuracy”), with the MBTR model’s mean absolute error of 0.6 kcal/mol corresponding to thermal fluctuations at room temperature. Note that MBTR achieves similar performance with a linear regression model, allowing constant-time predictions.

### Changes in crystal chemistry

Interpolation across changes in the chemistry of crystalline solids is demonstrated for a dataset of 11 k elpasolite structures ( $\text{ABC}_2\text{D}_6$ ,  $\text{AlNaK}_2\text{F}_6$  prototype) [56, 57]

composed of 12 different elements, with geometries and energies computed at DFT/PBE level of theory. Predicting formation energies with MBTR yields a root-mean-squared-error (RMSE) of 8.1 meV/atom and mean absolute error (MAE) of 4.7 meV/atom (Figure 2) for a training set of 9k crystals.

Adding chemical elements should increase the intrinsic dimensionality of the learning problem, and thus prediction errors. To verify this, we created a dataset of 4611

TABLE I: *Prediction errors for small organic molecules.* Machine-learning models of atomization energies  $E$  and isotropic polarizabilities  $\alpha$ , obtained at hybrid density functional level of theory, were trained on 5 k molecules and evaluated on 2 k others using different representations. RMSE=root mean square error, MAE=mean absolute error, CM=Coulomb matrix, BoB=bag of bonds, BAML=bonding angular machine learning, SOAP=smooth overlap of atomic positions, FCHL19=Faber-Christensen-Huang-Lilienfeld representation, MBTR=many-body tensor representation.

Representation	Kernel	$E / \text{kcal mol}^{-1}$		$\alpha / \text{\AA}^3$	
		MAE	RMSE	MAE	RMSE
CM [6]	Laplacian	3.47	4.76	0.13	0.17
BoB [23]	Laplacian	1.78	2.86	0.09	0.12
BAML [42]	Laplacian	1.15	2.54	0.07	0.12
SOAP [55]	REMatch	0.92	1.61	0.05	0.07
FCHL19 [45,47]	Gaussian	0.44	—	—	—
MBTR	Linear	0.74	1.14	0.07	0.10
MBTR	Gaussian	0.60	0.97	0.04	0.06

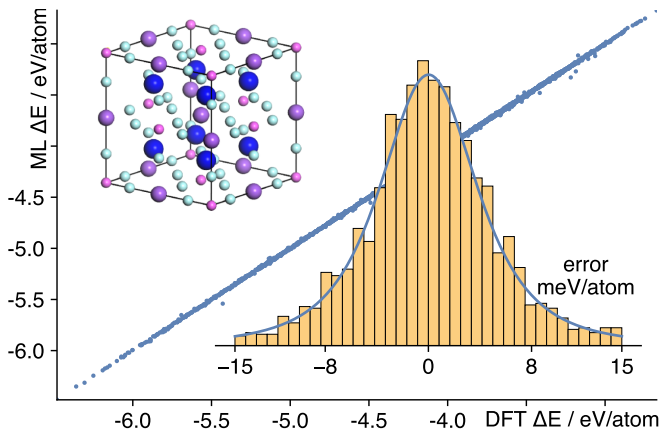


FIG. 2: Formation energy predictions for  $ABC_2D_6$  elpasolite structures containing 12 different elements. Shown are reference energies (DFT  $\Delta E$ ) and predicted energies (ML  $\Delta E$ ), as well as distribution of errors (inset) for 2272 crystals, from an MBTR machine learning model trained on 9086 other ones.

$ABC_2$  ternary alloys containing 22 non-radioactive elements from groups 1, 2, 13–15, spanning five rows and columns of the periodic table. Structures were taken from the Open Quantum Materials Database (OQMD) [58, 59], with geometries and properties also computed via DFT/PBE. As expected, energy predictions exhibit larger errors (RMSE 31 meV/atom, MAE 23 meV/atom) compared to an elpasolite model of same training set size (RMSE 23 meV/atom, MAE 15 meV/atom).

### Changes in molecular geometry

For interpolation of changes in molecular geometry, we employ a benchmark dataset [13,62] of ab initio molecular dynamics trajectories of eight organic molecules. Each molecule was simulated at a temperature of 500 K for between 150 k to 1 M time steps of 0.5 fs, with energies and forces computed at the DFT/PBE level of theory and the Tkatchenko–Scheffler model [63] for van der Waals interactions. Table II presents results for models trained and evaluated only on energies (right-hand side) and only on forces (left-hand side).

Energy-only models were trained on 10k configurations and validated on 2k other ones, employing MBTR (parametrized for dynamics data, see supplement) and a similarly modified CM ( $CM^{md}$ , see supplement). Non-linear MBTR regression performs best overall, with the linear kernel again being competitive.

On the one hand, differentiating energy-based machine learning potentials can introduce errors, for example, from small oscillations between training samples due to insufficient regularization, and from insufficient model constraints in directions not covered by the training data [64]. On the other hand, electronic structure calculations often provide reference forces at not additional cost. It is therefore beneficial to include these in model training. This often reduces the required number of reference calculations by an order of magnitude. [9,13,61,65]

Force-only models require an adaptation of plain KRR. To accommodate forces into training and to demonstrate use of MBTR with other regression approaches, we em-

ploy MBTR in the framework of symmetrized gradient-domain machine-learning (sGDML) [61]. This approach uses the Matérn kernel, augmentation by symmetric molecular permutations, and reference forces for training, while providing energy and force predictions.

Table II (left-hand side) compares performance of the original sGDML approach (based on the  $CM^{md}$  representation [13,61]) and of sGDML based on a 2-body MBTR representation. Both models were trained on 1000 configurations, leading to kernel matrices with dimensionalities between 27 k and 63 k. For reference, we also present results for the Faber-Christensen-Huang-Lilienfeld (FCHL) representation [45,47] and the polarizable atom interaction neural network (PaiNN) [60].

sGDML/MBTR performs as good or better than sGDML/ $CM^{md}$  for energy and force predictions. Compared to PaiNN, sGDML/MBTR performs better for energy predictions, but worse for forces. For a more fine-grained comparison between the sGDML models, Figure 3 presents learning curves of relative MAE ratios of sGDML/MBTR over sGDML/ $CM^{md}$ , together with standard deviations over five runs starting from different random seeds. sGDML/MBTR consistently outperforms sGDML/ $CM^{md}$  with error reductions up to 50%–60%, especially when less than 100 training samples are used. For more symmetric molecules such as benzene, malonaldehyde, and ethanol, use of MBTR is less beneficial but still an improvement.

### Phase diagrams

We demonstrate applicability by identifying the convex hull of the phase diagram for Pt-group/transition metal binary alloys, relevant for industrial applications [66]. For a given dataset of candidate structures, we predict the energy of each structure and identify those with the lowest energy, which form the convex hull in a phase diagram. Compositions that lie on or slightly above the convex hull correspond to stable and meta-stable alloys, respectively.

To demonstrate this, we use a dataset [66] of 153 alloys computed at the DFT/PBE level of theory. This dataset contains at most a few hundred structures for each alloy. Due to this small amount of data direct application of ML models results in errors in predicted energies that are large enough to lead to wrong convex hulls. We address this by employing a simple active learning [67] scheme:

Starting with a few randomly selected structures, we iteratively train ML models on these and predict energies of candidate structures. In each iteration, we calculate (look up) DFT energies only for structures predicted to be low in energy and include these in the training dataset of the next iteration. This procedure prevents computationally expensive DFT calculations for high-energy structures that lie above the convex hull, saving up to 48% of all DFT calculations while still identifying the correct convex hull.

Figure 4 presents results for AgPt. The active learning model selected 357 DFT calculations for training and predicted energies of 331 (48%) other structures, with a MAE of 39 meV/atom. The trade-off between the num-

TABLE II: *Energy and force prediction errors for changes in geometry of organic molecules.* Shown are prediction errors for total energies (kcal/mol) and atomic forces (kcal/mol/Å). MAE = mean absolute error, RMSE = root mean squared error, PaiNN = polarizable atom interaction neural network [60], FCHL19 = Faber-Christensen-Huang-Lilienfeld representation [45, 47], sGDML = symmetric gradient domain machine learning [13], sMatérn = Matérn kernel augmented with symmetric permutations for sGDML [61], CM<sup>md</sup> = Coulomb matrix variant, MBTR = many-body tensor representation.

Kernel	Trained only on forces, 1 k refs.								Trained only on energies, 10 k refs.		
	PaiNN		FCHL19 Gaussian		sGDML/CM <sup>md</sup> sMatérn		sGDML/MBTR sMatérn		CM <sup>md</sup> Gaussian	MBTR linear	MBTR Gaussian
	Energy MAE	Force MAE	Energy MAE	Force MAE	Energy MAE	Force MAE	Energy MAE	Force MAE	Energy MAE	Energy MAE	Energy MAE
benzene	—	—	—	—	0.07 <sup>a</sup>	0.06 <sup>a</sup>	0.07	0.15	0.03	0.03	0.03
uracil	0.11	0.13	0.10	0.10	0.11	0.24	0.11	0.17	0.05	0.10	0.03
naphthalene	0.12	0.08	0.12	0.15	0.12	0.11	0.11	0.09	0.12	0.10	0.07
aspirin	0.17	0.34	0.17	0.50	0.19	0.68	0.17	0.48	0.36	0.21	0.25
salicylic acid	0.12	0.20	0.12	0.22	0.12	0.28	0.11	0.18	0.11	0.13	0.07
malonaldehyde	0.10	0.34	0.08	0.25	0.10	0.41	0.09	0.36	0.18	0.21	0.10
ethanol	0.06	0.22	0.05	0.14	0.07	0.33	0.06	0.26	0.17	0.17	0.06
toluene	0.10	0.09	0.10	0.20	0.10	0.14	0.09	0.13	0.16	0.11	0.10

<sup>a</sup> We observed higher noise in predictions of benzene, whose reported prediction errors are also inconsistent in different publications. To make results comparable, we retrained the sGDML/CM<sup>md</sup> model (originally reported values are 0.10 and 0.06).

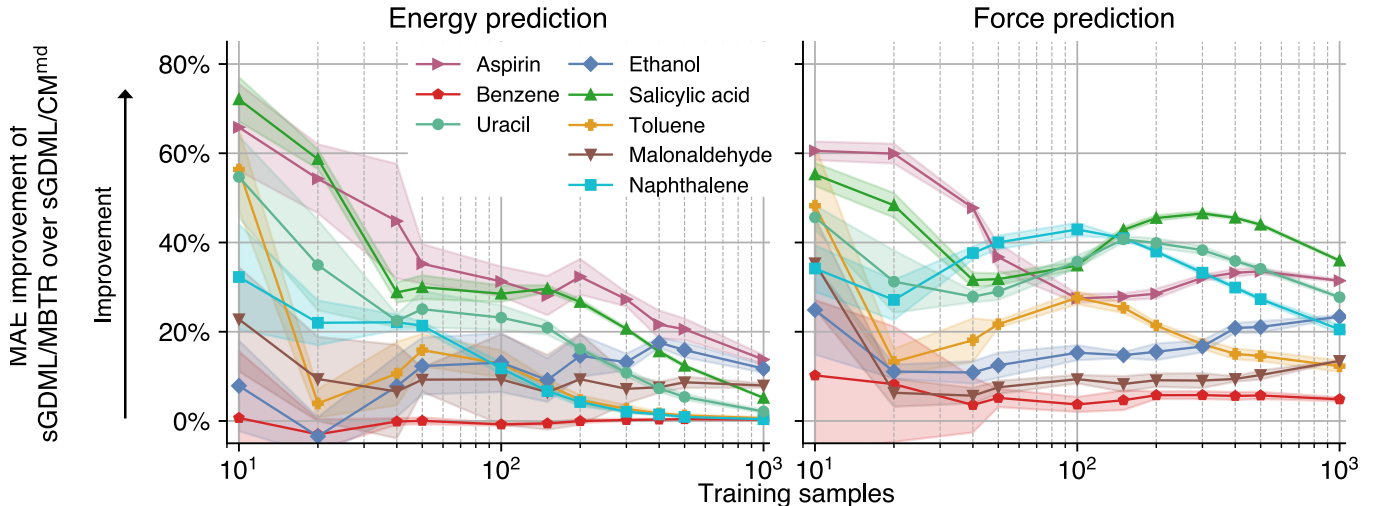


FIG. 3: *Relative improvement in predictive accuracy on dynamics data of eight different organic molecules.* Shown are force and energy prediction MAE ratios of sGDML/MBTR over sGDML/CM<sup>md</sup> as a function of training set size. Error bars show the standard deviation of the ratios over five runs with different random seeds.

ber of saved calculations and the probability of failing to identify the correct convex hull can be explicitly controlled by adjusting the energy threshold below which DFT calculations are requested. In this simple demonstration, structures are given and not derived from composition by relaxation. While structural relaxation is possible with ML, it brings its own challenges. [68–76]

#### Other uses

MBTR has been used to study structure and properties of molecules, clusters, crystals and other atomistic systems. Studies related to properties include predictions of

- gas-particle partition coefficients, such as saturation vapour pressure and equilibrium partitioning coefficients, of atmospheric molecules via kernel ridge regression [27]
- Heisenberg exchange spin coupling constants for dicop-

per complexes via Gaussian process regression [28]

- total and orbital energies of diverse larger organic molecules from the OE62 dataset [77] via a graph neural network [78]
- extrapolation of size-extensive properties [79] at the example of atomization energies of organic molecules in the QM9 [8] and OE62 [77] datasets
- formation energies of Al-Ni and Cd-Te binary compounds via support vector regression [34]
- band gaps and formation energies of perovskite-like materials [35]
- energetics of compositionally disordered compounds via kernel ridge regression [80]

Studies related to structure include

- visualization of the conformational space of tannic acid molecules via principal component analysis [29]

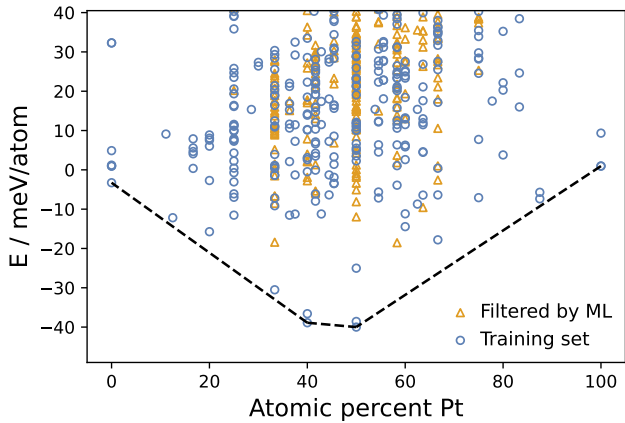


FIG. 4: Phase diagrams of Pt-group/transition metal binary alloys. Shown are  $\text{Ag}_x\text{Pt}_{1-x}$  structures (points) and their convex hull (dashed line) as given by DFT and identified by ML. All structures are shown at their DFT energy. Symbols indicate whether a structure was selected for training (blue circles) or predicted as high-energy (orange triangles). See main text for details.

- global optimization of atomic clusters, including electronic spin multiplicities, via active learning and Gaussian process regression [30,31]
- derivative-free structural relaxation of water and small unbranched alkanes via kernel ridge regression and simulated annealing [32]
- identification of low-energy point defects in solids via evolutionary algorithms, clustering, and Gaussian process regression [36]
- Monte Carlo simulations of the thermodynamics of thiolate-protected gold nanoclusters via minimal learning machine regression [37]
- developing data-efficient machine-learning potentials at the example of  $\text{Cs}^+$  in water via active learning and Gaussian process regression. [33]

## DISCUSSION AND OUTLOOK

MBTR is a general representation (numerical description, feature set) of atomistic systems for fast accurate interpolation between quantum-mechanical calculations via ML. It is based on distributions of  $k$ -atom terms stratified by chemical elements. Despite, or because of, this simple principle, it is connected to many other representations, including CM [6], BoB [23], histograms of distances, angles and dihedral angles [26], atom-centered symmetry functions [25], partial radial distribution functions [81], Faber-Christensen-Huang-von Lilienfeld representation [45,47], as well as cluster expansion [82]. See Ref. 16 for further details on these and other relationships.

MBTR represents whole molecules and crystals. With increasing number of atoms, and thus degrees of freedom, this approach is likely to degrade, and exploitation of locality via prediction of additive atomic energy contributions becomes appealing. [9,83] This requires representing local chemical environments [20], for which MBTR can be modified [34,84,85].

We note in passing that problems in the training of ML models, such as outliers, can often be traced back to problems in the underlying reference calculations, such as unconverged fast Fourier transform grids or inconsistent settings (violating the assumption that a single function is being fitted), a phenomenon also observed by others. [86] This suggests that automated identification of errors in big datasets of electronic structure calculations via parametrization of ML models might be a general approach for validation of such datasets. We rationalize this hypothesis by ML models identifying regularity (correlations) in data, and faulty calculations deviating in some way from correct ones.

Continuing advances in electronic structure codes and increasing availability of large-scale computing resources have led to large collections of ab initio calculations, such as Materials Project [87], AFLOWlib [88], Open Quantum Materials Database [59], and Novel Materials Discovery Laboratory [89]. Representations such as MBTR are key to combine quantum mechanics with machine learning (QM/ML) for fast, accurate and precise interpolation in these settings.

**Acknowledgments** MR and HH thank Matthias Scheffler for helpful discussions and support. MR thanks the Institute for Pure and Applied Mathematics (IPAM) for hospitality and support, participants of its program on Understanding Many-Particle Systems with Machine Learning for feedback, and Albert Bartók-Pártay, Gábor Csányi, Alexander Shapeev, Alexandre Tkatchenko and the late Alessandro de Vita for extended discussions. MR acknowledges funding from EU Horizon 2020 program grant 676580, The Novel Materials Discovery (NOMAD) Laboratory, a European Center of Excellence.

This article is an extended and updated version of the original arXiv preprint 1704.06439, whose formal publication was delayed for non-technical reasons.

**Data and Code Availability** All datasets used in this study are publicly available. Implementations of MBTR are available as part of the DScribe [85] and qmmlpack [90] libraries. Code to reproduce results of reported experiments is available at [github.com/hhaoyan/mbtr](https://github.com/hhaoyan/mbtr).

- \* Electronic address: [mrupp@mrupp.info](mailto:mrupp@mrupp.info); URL: [www.mrupp.info](http://www.mrupp.info)
- [1] Zoubin Ghahramani. Probabilistic machine learning and artificial intelligence. *Nature*, 521(7553):452–459, 2015. doi 10.1038/nature14541.
  - [2] Michael I. Jordan and Tom M. Mitchell. Machine learning: Trends, perspectives, and prospects. *Science*, 349(6245):255–260, 2015. doi 10.1126/science.aaa8415.
  - [3] Ryosuke Jinnouchi, Ferenc Karsai, and Georg Kresse. On-the-fly machine learning force field generation: Application to melting points. *Phys. Rev. B*, 100(1):014105, 2019. doi 10.1103/physrevb.100.014105.
  - [4] Austin D. Sendek, Ekin D. Cubuk, Evan R. Antoniuk, Gowoon Cheon, Yi Cui, and Evan J. Reed. Machine learning-assisted discovery of solid Li-ion conducting materials. *Chem. Mater.*, 31(2):342–352, 2019. doi 10.1021/acs.chemmater.8b03272.
  - [5] Raghunathan Ramakrishnan, Pavlo O. Dral, Matthias Rupp, and O. Anatole von Lilienfeld. Big data meets quantum chemistry approximations: The  $\Delta$ -machine learning approach. *J. Chem. Theor. Comput.*, 11(5):2087–2096, 2015. doi 10.1021/acs.jctc.5b00099.
  - [6] Matthias Rupp, Alexandre Tkatchenko, Klaus-Robert Müller, and O. Anatole von Lilienfeld. Fast and accurate modeling of molecular atomization energies with machine learning. *Phys. Rev. Lett.*, 108(5):058301, 2012. doi 10.1103/PhysRevLett.108.058301.
  - [7] Matthias Rupp. Machine learning for quantum mechanics in a nutshell. *Int. J. Quant. Chem.*, 115(16):1058–1073, 2015. doi 10.1002/qua.24954.
  - [8] Raghunathan Ramakrishnan, Pavlo O. Dral, Matthias Rupp, and O. Anatole von Lilienfeld. Quantum chemistry structures and properties of 134 kilo molecules. *Sci. Data*, 1:140022, 2014. doi 10.1038/sdata.2014.22.
  - [9] Albert P. Bartók, Mike C. Payne, Risi Kondor, and Gábor Csányi. Gaussian approximation potentials: The accuracy of quantum mechanics, without the electrons. *Phys. Rev. Lett.*, 104(13):136403, 2010. doi 10.1103/PhysRevLett.104.136403.
  - [10] Matthias Rupp, Raghunathan Ramakrishnan, and O. Anatole von Lilienfeld. Machine learning for quantum mechanical properties of atoms in molecules. *J. Phys. Chem. Lett.*, 6(16):3309–3313, 2015. doi 10.1021/acs.jpcllett.5b01456.
  - [11] Albert P. Bartók, Michael J. Gillan, Frederick R. Manby, and Gábor Csányi. Machine-learning approach for one- and two-body corrections to density functional theory: Applications to molecular and condensed water. *Phys. Rev. B*, 88(5):054104, 2013. doi 10.1103/PhysRevB.88.054104.
  - [12] Matthias Rupp. Machine learning for quantum mechanics in a nutshell. *Int. J. Quant. Chem.*, 115(16):1058–1073, 2015. doi 10.1002/qua.24954.
  - [13] Stefan Chmiela, Alexandre Tkatchenko, Huziel E. Sauceda, Igor Poltavsky, Kristof Schütt, and Klaus-Robert Müller. Machine learning of accurate energy-conserving molecular force fields. *Sci. Adv.*, 3(5):e1603015, 2017. doi 10.1126/sciadv.1603015.
  - [14] Volker L. Deringer, Albert P. Bartók, Noam Bernstein, David M. Wilkins, Michele Ceriotti, and Gábor Csányi. Gaussian process regression for materials and molecules. *Chem. Rev.*, 121(16):10073–10141, 2021. doi 10.1021/acs.chemrev.1c00022.
  - [15] Oliver T. Unke, Stefan Chmiela, Huziel E. Sauceda, Michael Gastegger, Igor Poltavsky, Kristof T. Schütt, Alexandre Tkatchenko, and Klaus-Robert Müller. Machine learning force fields. *Chem. Rev.*, 121(16):10142–10186, 2021. doi 10.1021/acs.chemrev.0c01111.
  - [16] Marcel F. Langer, Alex Goeßmann, and Matthias Rupp. Representations of molecules and materials for interpolation of quantum-mechanical simulations via machine learning. *npj Comput. Mater.*, 8:41, 2022. doi 10.1038/s41524-022-00721-x.
  - [17] Kernel methods use a positive definite function (kernel) to implicitly define the Hilbert space. We focus on explicit numerical representations as input for vector kernels.
  - [18] Jonathan E. Moussa. Comment on “Fast and accurate modeling of molecular atomization energies with machine learning”. *Phys. Rev. Lett.*, 109(5):059801, 2012. doi 10.1103/PhysRevLett.109.059801.
  - [19] Christopher R. Collins, Geoffrey J. Gordon, O. Anatole von Lilienfeld, and David J. Yaron. Constant size descriptors for accurate machine learning models of molecular properties. *J. Chem. Phys.*, 148(24):241718, 2018. doi 10.1063/1.5020441.
  - [20] Albert P. Bartók, Risi Kondor, and Gábor Csányi. On representing chemical environments. *Phys. Rev. B*, 87(18):184115, 2013. doi 10.1103/PhysRevB.87.184115.
  - [21] O. Anatole von Lilienfeld, Raghunathan Ramakrishnan, Matthias Rupp, and Aaron Knoll. Fourier series of atomic radial distribution functions: A molecular fingerprint for machine learning models of quantum chemical properties. *Int. J. Quant. Chem.*, 115(16):1084–1093, 2015. doi 10.1002/qua.24912.
  - [22] Berk Onat, Christoph Ortner, and James R. Kermode. Sensitivity and dimensionality of atomic environment representations used for machine learning interatomic potentials. *J. Chem. Phys.*, 153(14):144106, 2020. doi 10.1063/5.0016005.
  - [23] Katja Hansen, Franziska Biegler, Raghunathan Ramakrishnan, Wiktor Pronobis, O. Anatole von Lilienfeld, Klaus-Robert Müller, and Alexandre Tkatchenko. Machine learning predictions of molecular properties: Accurate many-body potentials and nonlocality in chemical space. *J. Phys. Chem. Lett.*, 6:2326–2331, 2015. doi 10.1021/acs.jpcllett.5b00831.
  - [24] Roberto Todeschini and Viviana Consonni. *Handbook of Molecular Descriptors*. Wiley, Weinheim, Germany, 2nd edition, 2009.
  - [25] Jörg Behler and Michele Parrinello. Generalized neural-network representation of high-dimensional potential-energy surfaces. *Phys. Rev. Lett.*, 98(14):146401, 2007. doi 10.1103/PhysRevLett.98.146401.
  - [26] Felix A. Faber, Luke Hutchison, Bing Huang, Justin Gilmer, Samuel S. Schoenholz, George E. Dahl, Oriol Vinyals, Steven Kearnes, Patrick F. Riley, and O. Anatole von Lilienfeld. Prediction errors of molecular machine learning models lower than hybrid DFT error. *J. Chem. Theor. Comput.*, 13(11):5255–5264, 2017. doi 10.1021/acs.jctc.7b00577.
  - [27] Emma Lumiaro, Milica Todorović, Theo Kurten, Hanna Vehkamäki, and Patrick Rinke. Predicting gas-particle partitioning coefficients of atmospheric molecules with machine learning. *Atmos. Chem. Phys.*, 21(17):13227–13246, 2021. doi 10.5194/acp-21-13227-2021.
  - [28] Marc Philipp Bahlke, Natnael Mogos, Jonny Proppe, and Carmen Herrmann. Exchange spin coupling from Gaussian process regression. *J. Phys. Chem. A*, 124(42):8708–8723, 2020. doi 10.1021/acs.jpca.0c05983.
  - [29] Romana Petry, Bruno Focassio, Gabriel R. Schleder, Diego Stéfani T. Martinez, and Adalberto Fazzio. Conformational analysis of tannic acid: Environment effects in electronic and reactivity properties. *J. Chem. Phys.*,

- 154(22):224102, 2021. doi 10.1063/5.0045968.
- [30] Maicon Pierre Lourenço, Lizandra Barrios Herrera, Jiří Hostaš, Patrizia Calaminici, Andreas M. Köster, Alain Tchagang, and Dennis R. Salahub. Taking the multiplicity inside the loop: active learning for structural and spin multiplicity elucidation of atomic clusters. *Theoretical Chemistry Accounts*, 140(8):116, 2021. doi 10.1007/s00214-021-02820-2.
- [31] Maicon Pierre Lourenço, Breno R. L. Galvão, Lizandra Barrios Herrera, Jiří Hostaš, Alain Tchagang, Mateus X. Silva, and Dennis R. Salahub. A new active learning approach for global optimization of atomic clusters. *Theoretical Chemistry Accounts*, 140(6):62, 2021. doi 10.1007/s00214-021-02766-5.
- [32] Eldhose Iype and Siddhaling Urolagin. Machine learning model for non-equilibrium structures and energies of simple molecules. *J. Chem. Phys.*, 150(2):024307, 2019. doi 10.1063/1.5054968.
- [33] Yaoguang Zhai, Alessandro Caruso, Sicun Gao, and Francesco Paesani. Active learning of many-body configuration space: Application to the  $\text{Cs}^+$ -water MB-nrg potential energy function as a case study. *J. Chem. Phys.*, 152(14):144103, 2020. doi 10.1063/5.0002162.
- [34] Shreyas J. Honrao, Stephen R. Xie, and Richard G. Hennig. Augmenting machine learning of energy landscapes with local structural information. *J. Appl. Phys.*, 128(8):085101, 2020. doi 10.1063/5.0012407.
- [35] Felix Mayr and Alessio Gagliardi. Global property prediction: A benchmark study on open-source, perovskite-like datasets. *ACS Omega*, 6(19):12722–12732, 2021. doi 10.1021/acsomega.1c00991.
- [36] Marco Arrigoni and Georg K. H. Madsen. Evolutionary computing and machine learning for discovering of low-energy defect configurations. *npj Comput. Mater.*, 7(1):71, 2021. doi 10.1038/s41524-021-00537-1.
- [37] Antti Pihlajamäki, Joonas Hämäläinen, Joakim Linja, Paavo Nieminen, Sami Malola, Tommi Kärkkäinen, and Hannu Häkkinen. Monte Carlo simulations of  $\text{Au}_{38}(\text{SCH}_3)_{24}$  nanocluster using distance-based machine learning methods. *J. Phys. Chem. A*, 124(23):4827–4836, 2020. doi 10.1021/acs.jpca.0c01512.
- [38] Grégoire Montavon, Matthias Rupp, Vivekanand Gobre, Alvaro Vazquez-Mayagoitia, Katja Hansen, Alexandre Tkatchenko, Klaus-Robert Müller, and O. Anatole von Lilienfeld. Machine learning of molecular electronic properties in chemical compound space. *New J. Phys.*, 15(9):095003, 2013. doi 10.1088/1367-2630/15/9/095003.
- [39] Luca M. Ghiringhelli, Jan Vybiral, Sergey V. Levchenko, Claudia Draxl, and Matthias Scheffler. Big data of materials science: Critical role of the descriptor. *Phys. Rev. Lett.*, 114(10):105503, 2015. doi 10.1103/PhysRevLett.114.105503.
- [40] Sergey N. Pozdnyakov, Michael J. Willatt, Albert P. Bartók, Christoph Ortner, Gábor Csányi, and Michele Ceriotti. Incompleteness of atomic structure representations. *Phys. Rev. Lett.*, 125(16):166001, 2020. doi 10.1103/physrevlett.125.166001.
- [41] Ekin D. Cubuk, Samuel S. Schoenholz, Jennifer M. Rieser, Brad D. Malone, Joerg Rottler, Douglas J. Durian, Efthimios Kaxiras, and Andrea J. Liu. Identifying structural flow defects in disordered solids using machine-learning methods. *Phys. Rev. Lett.*, 114(10):108001, 2015. doi 10.1103/PhysRevLett.114.108001.
- [42] Bing Huang and O. Anatole von Lilienfeld. Communication: Understanding molecular representations in machine learning: the role of uniqueness and target similarity. *J. Chem. Phys.*, 145(16):161102, 2016. doi 10.1063/1.4964627.
- [43] Kun Yao, John E. Herr, and John Parkhill. The many-body expansion combined with neural networks. *J. Chem. Phys.*, 146(1):014106, 2017. doi 10.1063/1.4973380.
- [44] We use scalar geometry functions  $g_k$  for convenience; assigning vectors would simply increase the rank of the tensor. The product structure  $w_k(\mathbf{i})\mathcal{D}(x, g_k(\mathbf{i}))$  allows efficient implementation as  $\mathcal{D}$  does not depend on  $\mathcal{M}$ .
- [45] Felix A. Faber, Anders S. Christensen, Bing Huang, and O. Anatole von Lilienfeld. Alchemical and structural distribution based representation for universal quantum machine learning. *J. Chem. Phys.*, 148(24):241717, 2018. doi 10.1063/1.5020710.
- [46] John E. Herr, Kevin Koh, Kun Yao, and John Parkhill. Compressing physics with an autoencoder: Creating an atomic species representation to improve machine learning models in the chemical sciences. *J. Chem. Phys.*, 151(6–7):455–472, 2019. doi 10.1063/1.5108803.
- [47] Anders S. Christensen, Lars A. Bratholm, Felix A. Faber, and O. Anatole von Lilienfeld. FCHL revisited: Faster and more accurate quantum machine learning. *J. Chem. Phys.*, 152(4):044107, 2020. doi 10.1063/1.5126701.
- [48] Effectively representing one unit cell, including influence of surrounding cells on it, in accordance with computed properties being reported per cell.
- [49] Exponential weighting was motivated by the exponential decay of screened Coulombic interactions in solids.
- [50] Roy Frostig, Matthew James Johnson, and Chris Leary. Compiling machine learning programs via high-level tracing. In *1st Conference on Systems and Machine Learning (SysML 2018), Stanford, California, February 15–16*, 2018. URL <https://mlsys.org/Conferences/doc/2018/146.pdf>.
- [51] Adam Paszke, Sam Gross, Francisco Massa, Adam Lerer, James Bradbury, Gregory Chanan, Trevor Killeen, Zeming Lin, Natalia Gimelshein, Luca Antiga, Alban Desmaison, Andreas Kopf, Edward Yang, Zachary DeVito, Martin Raison, Alykhan Tejani, Sasank Chilamkurthy, Benoit Steiner, Lu Fang, Junjie Bai, and Soumith Chintala. PyTorch: An imperative style, high-performance deep learning library. In Hanna Wallach, Hugo Larochelle, Alina Beygelzimer, Florence d’Alché Buc, Emily Fox, and Roman Garnett, editors, *Advances in Neural Information Processing Systems 32 (NeurIPS 2019), Montréal, Canada, December 8–14*, pages 8024–8035. Curran Associates, 2019. URL <https://neurips.cc/Conferences/2019>.
- [52] John P. Perdew, Kieron Burke, and Matthias Ernzerhof. Generalized gradient approximation made simple. *Phys. Rev. Lett.*, 77(18):3865–3868, 1996. doi 10.1103/PhysRevLett.77.3865.
- [53] John P. Perdew, Matthias Ernzerhof, and Kieron Burke. Rationale for mixing exact exchange with density functional approximations. *J. Chem. Phys.*, 105(22):9982–9985, 1996.
- [54] Carlo Adamo and Vincenzo Barone. Toward reliable density functional methods without adjustable parameters: The PBE0 model. *J. Chem. Phys.*, 110(13):6158–6170, 1999. doi 10.1063/1.478522.
- [55] Sandip De, Albert P. Bartók, Gábor Csányi, and Michele Ceriotti. Comparing molecules and solids across structural and alchemical space. *Phys. Chem. Chem. Phys.*, 18(20):13754–13769, 2016. doi 10.1039/C6CP00415F.
- [56] Felix A. Faber, Alexander Lindmaa, O. Anatole von Lilienfeld, and Rickard Armiento. Machine learning energies of 2 million elpasolite ( $\text{ABC}_2\text{D}_6$ ) crystals. *Phys. Rev. Lett.*, 117(13):135502, 2016. doi 10.1103/PhysRevLett.117.135502.

- [57] Dataset ABC2D6-16, available at <http://qmml.org>.
- [58] James E. Saal, Scott Kirklin, Muratahan Aykol, Bryce Meredig, and Chris Wolverton. Materials design and discovery with high-throughput density functional theory: The open quantum materials database (OQMD). *J. Miner. Met. Mater. Soc.*, 65(11):1501–1509, 2013. doi 10.1007/s11837-013-0755-4.
- [59] Scott Kirklin, James E. Saal, Bryce Meredig, Alex Thompson, Jeff W. Doak, Muratahan Aykol, Stephan Rühl, and Chris Wolverton. The open quantum materials database (OQMD): assessing the accuracy of DFT formation energies. *npj Comput. Mater.*, 1:15010, 2015. doi 10.1038/npjcompumats.2015.10.
- [60] Kristof T. Schütt, Oliver T. Unke, and Michael Gastegger. Equivariant message passing for the prediction of tensorial properties and molecular spectra. In Marina Meila and Tong Zhang, editors, *Proceedings of the 38th International Conference on Machine Learning (ICML 2021), virtual, July 18–24*, pages 9377–9388. Proceedings of Machine Learning Research, 2021. URL <https://proceedings.mlr.press/v139/schutt21a.html>.
- [61] Stefan Chmiela, Huziel E. Sauceda, Klaus-Robert Müller, and Alexandre Tkatchenko. Towards exact molecular dynamics simulations with machine-learned force fields. *Nat. Commun.*, 9:3887, 2018. doi 10.1038/s41467-018-06169-2.
- [62] Kristof T. Schütt, Farhad Arbabzadah, Stefan Chmiela, Klaus R. Müller, and Alexandre Tkatchenko. Quantum-chemical insights from deep tensor neural networks. *Nat. Comm.*, 8:13890, 2017. doi 10.1038/ncomms13890.
- [63] Alexandre Tkatchenko and Matthias Scheffler. Accurate molecular van der Waals interactions from ground-state electron density and free-atom reference data. *Phys. Rev. Lett.*, 102(7):073005, 2009. doi 10.1103/PhysRevLett.102.073005.
- [64] John C. Snyder, Matthias Rupp, Katja Hansen, Klaus-Robert Müller, and Kieron Burke. Finding density functionals with machine learning. *Phys. Rev. Lett.*, 108(25):253002, 2012. doi 10.1103/PhysRevLett.108.253002.
- [65] Aldo Glielmo, Peter Sollich, and Alessandro De Vita. Accurate interatomic force fields via machine learning with covariant kernels. *Phys. Rev. B*, 95(21):214302, 2017. doi 10.1103/PhysRevB.95.214302.
- [66] Gus L.W. Hart, Stefano Curtarolo, Thaddeus B. Masalski, and Ohad Levy. Comprehensive search for new phases and compounds in binary alloy systems based on platinum-group metals, using a computational first-principles approach. *Phys. Rev. X*, 3:041035, 2013. doi 10.1103/PhysRevX.3.041035.
- [67] Burr Settles. *Active Learning*, volume 18 of *Synthesis Lectures on Artificial Intelligence and Machine Learning*. Morgan & Claypool, 2012. doi 10.2200/S00429ED1V01Y201207AIM018.
- [68] Zachary W. Ulissi, Aayush R. Singh, Charlie Tsai, and Jens K. Nørskov. Automated discovery and construction of surface phase diagrams using machine learning. *J. Phys. Chem. Lett.*, 7(19):3931–3935, 2016. doi 10.1021/acs.jpcclett.6b01254.
- [69] Esben L. Kolsbjerg, Andrew A. Peterson, and Bjørk Hammer. Neural-network-enhanced evolutionary algorithm applied to supported metal nanoparticles. *Phys. Rev. B*, 97(19):195424, 2018. doi 10.1103/PhysRevB.97.195424.
- [70] Alexander Denzel and Johannes Kästner. Gaussian process regression for geometry optimization. *J. Chem. Phys.*, 148(9):094114, 2018. doi 10.1063/1.5017103.
- [71] Gunnar Schmitz and Ove Christiansen. Gaussian process regression to accelerate geometry optimizations relying on numerical differentiation. *J. Chem. Phys.*, 148(24):241704, 2018. doi 10.1063/1.5009347.
- [72] Junwoong Yoon and Zachary W. Ulissi. Differentiable optimization for the prediction of ground state structures (DOGSS). *Phys. Rev. Lett.*, 125(17):173001, 2020. doi 10.1103/physrevlett.125.173001.
- [73] Henrik Lund Mortensen, Søren Ager Meldgaard, Malthe Kjær Bisbo, Mads-Peter V. Christiansen, and Bjørk Hammer. Atomistic structure learning algorithm with surrogate energy model relaxation. *Phys. Rev. B*, 102(7):075427, 2020. doi 10.1103/physrevb.102.075427.
- [74] Daniel Huang, Junwei Lucas Bao, and Jean-Baptiste Tristan. Geometry meta-optimization. *J. Chem. Phys.*, 156(13):134109, 2022. doi 10.1063/5.0087165.
- [75] Dongxiao Hao, Xibing He, Adrian E. Roitberg, Shengli Zhang, and Junmei Wang. Development and evaluation of geometry optimization algorithms in conjunction with ANI potentials. *J. Chem. Theor. Comput.*, 18(2):978–991, 2022. doi 10.1021/acs.jctc.1c01043.
- [76] Daniel Born and Johannes Kästner. Geometry optimization in internal coordinates based on Gaussian process regression: Comparison of two approaches. *J. Chem. Theor. Comput.*, 17(9):5955–5967, 2021. doi 10.1021/acs.jctc.1c00517.
- [77] Annika Stuke, Christian Kunkel, Dorothea Golze, Milica Todorović, Johannes T. Margraf, Karsten Reuter, Patrick Rinke, and Harald Oberhofer. Atomic structures and orbital energies of 61,489 crystal-forming organic molecules. *Sci. Data*, 17(2–4):83–92, 2020. doi 10.1038/s41597-020-0385-y.
- [78] Obaidur Rahaman and Alessio Gagliardi. Deep learning total energies and orbital energies of large organic molecules using hybridization of molecular fingerprints. *J. Chem. Inf. Model.*, 60(12):5971–5983, 2020. doi 10.1021/acs.jcim.0c00687.
- [79] Hyunwook Jung, Sina Stocker, Christian Kunkel, Harald Oberhofer, Byungchan Han, Karsten Reuter, and Johannes T. Margraf. Size-extensive molecular machine learning with global representations. *ChemSystemChem*, 2(4):e1900052, 2020. doi 10.1002/syst.201900052.
- [80] Mostafa Yaghoobi and Mojtaba Alaei. Machine learning for compositional disorder: A comparison between different descriptors and machine learning frameworks. *Comput. Mater. Sci.*, 207:111284, 2022. doi 10.1016/j.commatsci.2022.111284.
- [81] Kristof T. Schütt, Henning Glawe, Felix Brockherde, Antonio Sanna, Klaus-Robert Müller, and Eberhard K.U. Gross. How to represent crystal structures for machine learning: Towards fast prediction of electronic properties. *Phys. Rev. B*, 89(20):205118, 2014. doi 10.1103/PhysRevB.89.205118.
- [82] Juan M. Sanchez, François Ducastelle, and Denis Gratias. Generalized cluster description of multicomponent systems. *Phys. Stat. Mech. Appl.*, 128(1–2):334–350, 1984. doi 10.1016/0378-4371(84)90096-7.
- [83] Jörg Behler. Neural network potential-energy surfaces in chemistry: a tool for large-scale simulations. *Phys. Chem. Chem. Phys.*, 13(40):17930–17955, 2011. doi 10.1039/C1CP21668F.
- [84] Marc O. J. Jäger, Eiaki V. Morooka, Filippo Federici-Canova, Lauri Himanen, and Adam S. Foster. Machine learning hydrogen adsorption on nanoclusters through structural descriptors. *npj Comput. Mater.*, 4:37, 2018. doi 10.1038/s41524-018-0096-5.
- [85] Lauri Himanen, Marc O.J. Jäger, Eiaki V. Morooka, Filippo Federici-Canova, Yashasvi S. Ranawat, David Z. Gao, Patrick Rinke, and Adam S. Foster. DScribe: Li-

- brary of descriptors for machine learning in materials science. *Comput. Phys. Comm.*, 247:106949, 2019. doi 10.1016/j.cpc.2019.106949.
- [86] Independent personal communications by Jörg Behler, Gábor Csányi, and Ekin Doğuş Çubuk.
- [87] Anubhav Jain, Shyue Ping Ong, Geoffroy Hautier, Wei Chen, William Davidson Richards, Stephen Dacek, Shreyas Cholia, Dan Gunter, David Skinner, Gerbrand Ceder, and Kristin A. Persson. Commentary: The materials project: A materials genome approach to accelerating materials innovation. *APL Mater.*, 1:011002, 2013. doi 10.1063/1.4812323.
- [88] Stefano Curtarolo, Wahyu Setyawan, Gus L. W. Hart, Michal Jahnatek, Roman V. Chepulskii, Richard H. Taylor, Shidong Wang, Junkai Xue, Kesong Yang, Ohad Levy, Michael J. Mehl, Harold T. Stokes, Denis O. Demchenko, and Dane Morgan. AFLOW: An automatic framework for high-throughput materials discovery. *Comput. Mater. Sci.*, 58(6):218–226, 2012. doi 10.1016/j.commatsci.2012.02.005.
- [89] Claudia Draxl and Matthias Scheffler. The NOMAD laboratory: from data sharing to artificial intelligence. *J. Phys. Mater.*, 2(3):036001, 2019. doi 10.1088/2515-7639/ab13bb.
- [90] Available as part of the software **qmmlpack** (quantum mechanics machine learning package) at <https://gitlab.com/qmml/qmmlpack> under the Apache 2.0 license.

# Supplementary Material

## Unified Representation of Molecules and Crystals for Machine Learning

Haoyan Huo,<sup>1,2</sup> Matthias Rupp<sup>3,4,5\*</sup>

<sup>1</sup> School of Physics, Peking University, Beijing, People’s Republic of China

<sup>2</sup> Present address: Department of Materials Science and Engineering, University of California, Berkeley, CA, USA

<sup>3</sup> Fritz Haber Institute of the Max Planck Society, Berlin, Germany

<sup>4</sup> Department of Computer and Information Science, University of Konstanz, Konstanz, Germany

<sup>5</sup> Present address: Materials Research and Technology Department, Luxembourg Institute of Science and Technology (LIST), Belvaux, Luxembourg

\* [mrupp@mrupp.info](mailto:mrupp@mrupp.info); [www.mrupp.info](http://www.mrupp.info)

### S1 Parametrization of MBTR

Table S1 lists all parametrizations of MBTR used in the study.

Table S1: *Parametrizations of MBTR* used. In all experiments,  $\mathcal{D}$  was the normal distribution with standard deviation  $\sigma$  and element correlation matrices were identity matrices,  $\mathbf{C}_{\alpha,\beta} = \delta_{\alpha=\beta}$ . Symbol  $\sigma^*$  indicates that  $\sigma$  is dataset-dependent and must be optimized.  $\mathbf{R}_a, \mathbf{R}_b, \dots$  are Cartesian coordinates of many-body atomistic N-body systems  $\mathcal{M}_a, \mathcal{M}_b, \dots$ , and,  $\mathbf{p} = \mathbf{R}_a - \mathbf{R}_b, \mathbf{q} = \mathbf{R}_c - \mathbf{R}_a, \mathbf{r} = \mathbf{R}_b - \mathbf{R}_c$ , with norms  $p = \|\mathbf{p}\|, q = \|\mathbf{q}\|, r = \|\mathbf{r}\|$ . EIF = element indexing function, AIF = atom indexing function. Full indexing and the non-reversal (N.R.) indexing function are described in Section S3

Experiment	$k$	$x_{\min}$	$\Delta x$	$d$	$\sigma$	$g$	$w$	EIF	AIF
Fig. 1 (left)	2	0	$2.20441 \cdot 10^{-3}$	500	$2^{-4.5}$	$p^{-1}$	$p^{-2}$	full	full
Fig. 1 (right)	3	-1.178	$4.712 \cdot 10^{-3}$	500	0.04	$\cos \angle(\mathbf{p}, -\mathbf{r})$	$\exp(-\frac{pqr}{\sigma_w})$	full	full
Table. 1 $E$	2	0.1	$1.1 \cdot 10^{-2}$	100	$\sigma^*$	$p^{-1}$	$p^{-2}$	N.R.	N.R.
	3	-0.15	$3.45575 \cdot 10^{-2}$	100	$\sigma^*$	$\angle(\mathbf{p}, -\mathbf{r})$	$\frac{1}{pqr}$	N.R.	N.R.
Table. 1 $\alpha$	1	-0.5	$\frac{17}{30}$	30	$\sigma^*$	count	1	full	full
	2	0.1	$1.1 \cdot 10^{-2}$	100	$\sigma^*$	$p^{-1}$	$p^{-2}$	N.R.	N.R.
	3	-0.15	$3.456 \cdot 10^{-2}$	100	$\sigma^*$	$\angle(\mathbf{p}, -\mathbf{r})$	$\frac{1}{pqr}$	N.R.	N.R.
Fig. 2 ( $ABC_2D_6$ )	1	-0.5	$\frac{7}{30}$	30	$\sigma^*$	count	1	full	full
	2	-0.07	$7.9 \cdot 10^{-3}$	100	$\sigma^*$	$p^{-1}$	$p^{-2}$	N.R.	N.R.
$ABC_2$ ternaries	1	-0.5	$\frac{3}{30}$	30	$\sigma^*$	count	1	full	full
	2	-0.07	$5.9 \cdot 10^{-3}$	100	$\sigma^*$	$p^{-1}$	$p^{-2}$	N.R.	N.R.
MD17 energy-only	2	$1.05d_{max}^{-1} - 0.05d_{min}^{-1}$	$d_{min}^{-1} - d_{max}^{-1}$	30	$\sigma^*$	$p^{-1}$	1	N.R.	N.R.
	3	-0.05 $\pi$	$\frac{1.1\pi}{30}$	30	$\sigma^*$	$\angle(\mathbf{p}, -\mathbf{r})$	1	N.R.	N.R.
MD17 sGDML	2	0	$8.5 \cdot 10^{-2}$	16	$\sigma^*$	$p^{-1}$	1	N.R.	N.R.
Phase diagrams	2	0	$5 \cdot 10^{-3}$	100	$\sigma^*$	$p^{-1}$	$p^{-2}$	N.R.	N.R.

### S2 Datasets

#### Molecular properties

**GDB7-13 (QM7b) dataset** [1] This is a modified version of the GDB7-12/QM7 dataset [2], with further relaxed geometries, 13 additional properties, and some Cl-containing molecules added. It contains 7 211 small organic molecules with up to 7 atoms of element types C, N, O, S, Cl, saturated with hydrogens. From the properties provided in the original reference, we retain the ground state properties at the highest level of theory provided. The properties and performances of different models are shown in Table S2.

Table S2: *Performance on GDB7-13 (QM7b) dataset.* (a) List of properties, level of theory of calculation, and mean and standard deviations of the properties across the entire dataset. (b) Performance of different models on predicting energy ( $E$ ) and isotropic polarizabilities ( $\alpha$ ). RMSE = root mean square error, MAE = mean absolute error, CM = Coulomb matrix, BoB = bag of bonds, BAML = bonding angular machine learning, SOAP = smooth overlap of atomic positions, MBTR = many-body tensor representation.

Property	Method	Unit	$\mu \pm \sigma$	Comment
$\mathbf{R}$	DFT/PBE	Å		equilibrium geometry
$E$	DFT/PBE0	kcal mol <sup>-1</sup>	-1 563 ± 224	atomization energy
$\alpha$	DFT/PBE0	Å <sup>3</sup>	11.11 ± 1.34	isotropic molecular polarizability
HOMO	GW	eV	-9.09 ± 0.70	highest occupied molecular orbital
LUMO	GW	eV	0.78 ± 0.48	lowest unoccupied molecular orbital

(a)

Repr.	Kernel	E / kcal mol <sup>-1</sup>		$\alpha$ / Å <sup>3</sup>	
		RMSE	MAE	RMSE	MAE
CM	Laplacian	5.48	3.54	0.18	0.13
BoB	Laplacian	3.32	1.95	0.13	0.09
BAML [3]	Laplacian	2.54	1.15	0.12	0.07
SOAP [4]	REMatch	1.61	0.92	0.07	0.05
MBTR	Linear	1.14	0.74	0.10	0.07
MBTR	Laplacian	3.50	2.31	0.09	0.06
MBTR	Gaussian	0.97	0.60	0.06	0.04

(b)

**Molecular dynamics of organic molecules, the MD17 dataset.** We used the MD17 dataset by Chmiela et al. [5] which contains 8 datasets of molecular dynamics trajectories and energy/force associated with each configuration. For training simple energy-only models, a modified variant of the Coulomb matrix is used. As the constituting atoms of a molecule and their order remain fixed throughout the simulation, there is no need for a sorting step, nor to encode element types as these are implicitly given by the atoms position in the matrix. The remaining representation simply encodes inverse distances:

$$\text{CM}_{i,j}^{\text{md}} = \begin{cases} \|\mathbf{R}_i - \mathbf{R}_j\|_2^{-1} & i \neq j \\ 0 & i = j \end{cases},$$

of which we use only the lower triangular part without the diagonal. Without the discontinuities from sorting, the smoother Gaussian kernel now performs better than the Laplacian kernel (Table S3).

For training sGDML force models using MBTR, we used the same sGDML method [6] which employed the Matérn kernel and symmetric permutations to atom positions, except that we replaced CM<sup>md</sup> representation with MBTR. Note that in these experiments, to make results comparable, each atom is also treated as its own chemical element type, as in computing CM<sup>md</sup>.

Table S3 shows the performance of different energy-only models trained on the MD17 dataset, extending Table II. Fig. S1 shows the learning curve of sGDML/MBTR models, i.e., MAE as functions of training dataset sizes for different MD17 datasets. To supplement Fig. 3 which only shows MAE improvements of sGDML/MBTR over sGDML/CM<sup>md</sup>, we also show the RMSE improvements in Fig. S2.

## Crystalline properties

**$ABC_2D_6$  and  $ABC_2$  energies.** Table. S4 shows the performance of MBTR models on both the  $ABC_2D_6$  and  $ABC_2$  crystals. Fig. S3 shows the learning curves, i.e., prediction errors of MBTR models as a function of training set size for both  $ABC_2D_6$  elpasolite and  $ABC_2$  ternary compounds. Training is done for both the complete dataset and with one/two/three chemical species removed. Note that due to the size of the dataset, training with 3 chemical species removed leads to too few data points for  $ABC_2D_6$  dataset, precluding a reliable estimation of the learning curve.

Table S3: Prediction errors of energy-only models for changes in geometry of small organic molecules. MBTR models were trained on 10k random frames from ab initio molecular dynamics simulations and evaluated on 2k other frames. Shown are root mean squared error (RMSE) and mean absolute errors (MAE) of total energies.

kcal / mol	CM <sup>md</sup> Gaussian		CM <sup>md</sup> Laplacian		MBTR linear		MBTR Gaussian		MBTR Laplacian	
	RMSE	MAE	RMSE	MAE	RMSE	MAE	RMSE	MAE	RMSE	MAE
benzene	0.043	0.031	0.307	0.230	0.046	0.034	0.036	0.026	0.282	0.207
uracil	0.079	0.054	0.919	0.671	0.128	0.096	0.047	0.031	0.758	0.534
naphthalene	1.158	1.119	1.422	1.093	0.125	0.095	0.093	0.068	1.160	0.875
aspirin	0.505	0.356	2.527	1.895	0.285	0.208	0.345	0.248	2.100	1.559
salicylic acid	0.155	0.110	1.382	1.057	0.174	0.127	0.102	0.068	1.193	0.900
malonaldehyde	0.246	0.176	1.279	0.963	0.283	0.211	0.142	0.097	1.125	0.834
ethanol	0.231	0.166	1.047	0.794	0.227	0.168	0.084	0.060	0.708	0.518
toluene	0.214	0.158	1.560	1.188	0.153	0.112	0.141	0.103	1.349	1.031

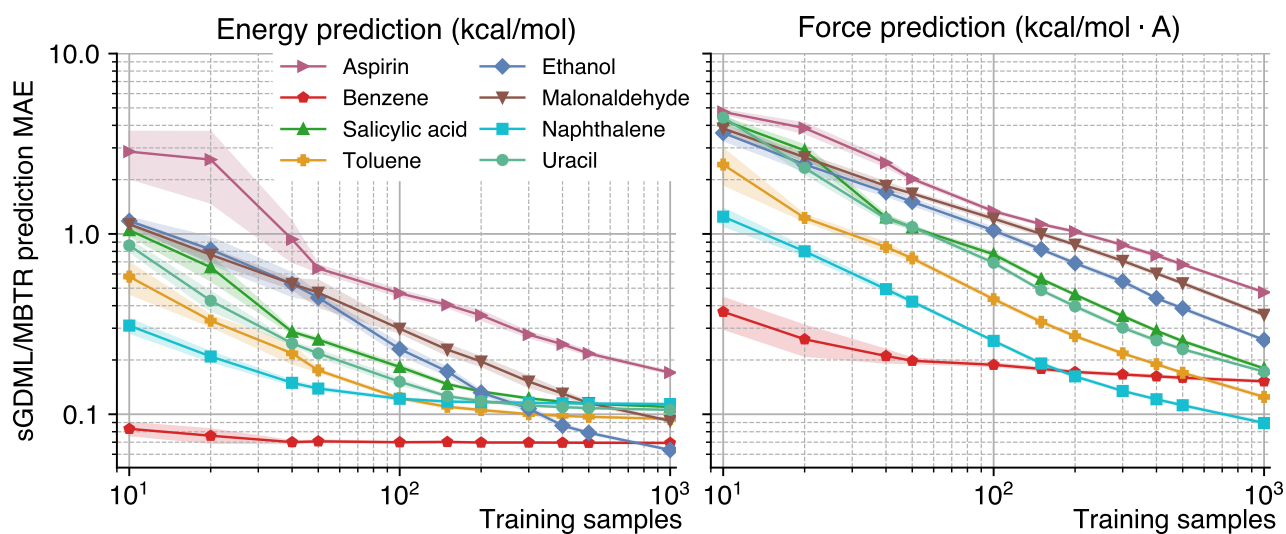


Figure S1: Learning curve of sGDML/MBTR for the MD17 dataset. Curves are estimated using results from 5 runs with different random seeds, and the shaded areas show estimated standard deviation of the curves.

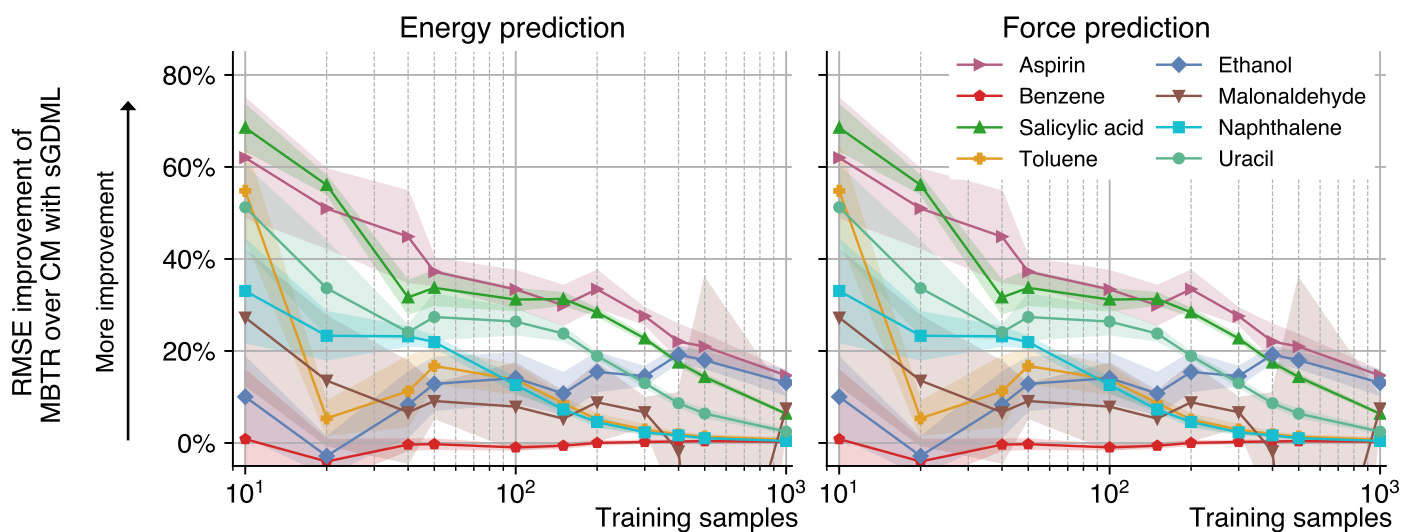


Figure S2: RMSE of prediction error improvements of MBTR over CM<sup>md</sup> on molecular dynamics predictions for the organic molecule dataset.

Table S4: Performance of crystalline energy prediction. for (a) 11k elpasolites and (b) 4.6k ternary compounds. RMSE = root mean square error, MAE = mean absolute error, MBTR = many-body tensor representation. Prediction errors are in meV/atom.

Training size		9086		3594	
Repr.	Kernel	RMSE	MAE	RMSE	MAE
MBTR	Linear	28	21	37	27
MBTR	Laplacian	11	6	29	18
MBTR	Gaussian	8	5	23	15

(a) 11k  $ABC_2D_6$  elpasolites.

Training size		3594	
Repr.	Kernel	RMSE	MAE
MBTR	Linear	55	38
MBTR	Laplacian	37	27
MBTR	Gaussian	31	23

(b) 4.6k  $ABC_2$  ternary compounds.

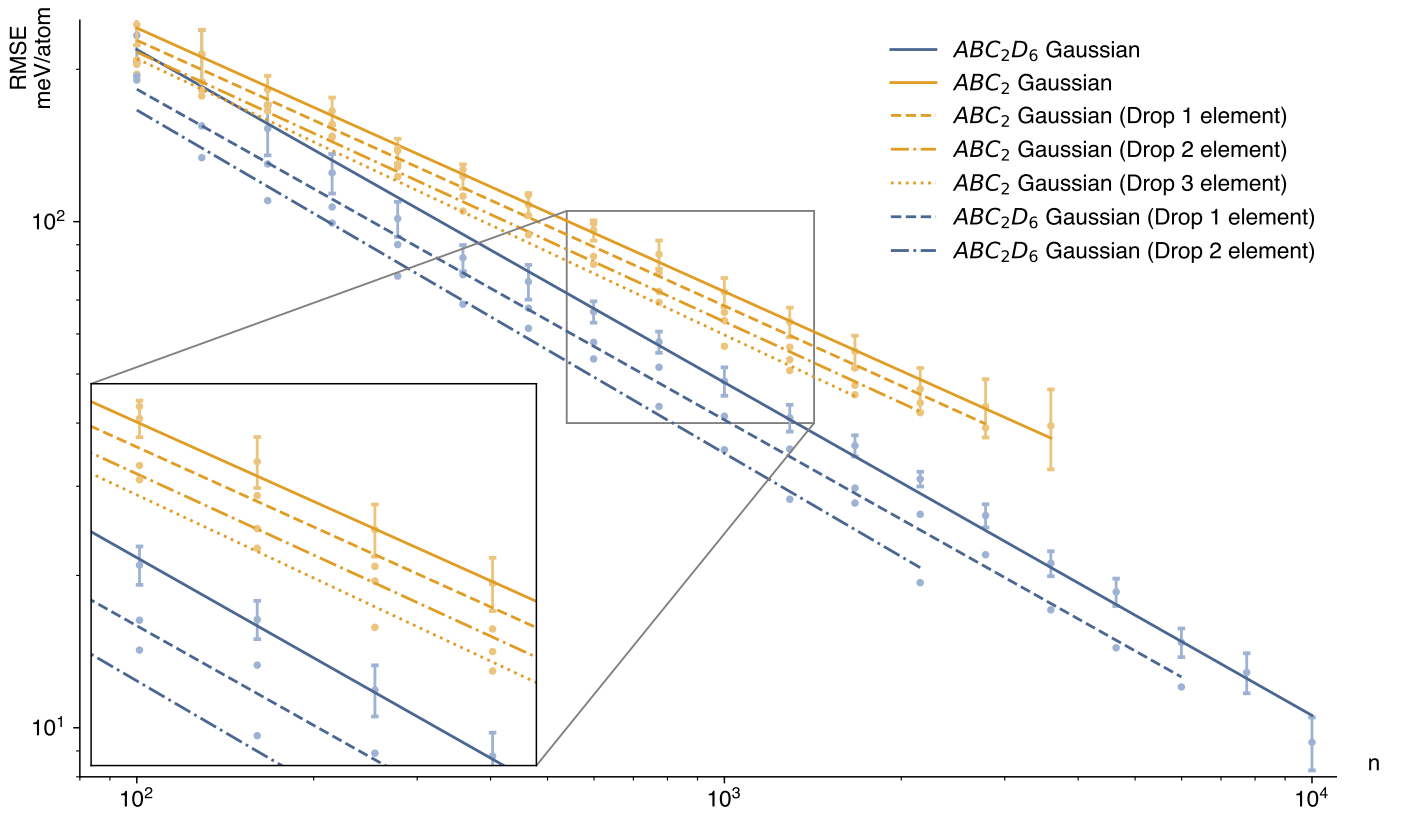


Figure S3: Learning curves for both  $ABC_2D_6$  elpasolite and  $ABC_2$  ternary datasets. Dots show experiment results of MBTR models trained using different training set sizes (X-axis) that achieve decreasing prediction errors (Y-axis). Lines are the fitted training curves (in log scale) whose slopes indicate how fast prediction errors are reduced with more training data.

## S3 Implementation

Discretized MBTR calculation benefits from two types of combinatorial enumeration, one for linearization of the tensor element dimensions and one for enumeration of  $k$ -tuples of atoms. The two differ with respect to repeated indices, which are required for elements (to include interactions between atoms of same element type), but are excluded for atoms (to avoid zero distances and undefined angles). For elements, our algorithm requires indexing functions that map an element tuple to its corresponding row in the linearized tensor. For atoms, no indexing is required.

### Tensor linearization

The  $k$  element dimensions of the MBTR can be linearized as all  $k$ -tuples with repetition over  $\{1, \dots, n\}$ , where  $n$  is the number of chemical elements in the data. Many choices of  $g$  obey invariants allowing removal of redundant tuples. For example, distances, angles, and torsional angles are invariant to reversal (the angle between atoms (1, 5, 2) and (2, 5, 1) is the same). In the following, we exclude reversed tuples and enumerate in lexicographic order. The latter is only a convention; any fixed order that allows identification of tensor elements later on would do.

### Size of MBTR

Let  $f_e(n, k)$  denote the number of  $k$ -tuples over  $\{1, \dots, n\}$  with repetition, but without reversals, that is, counting  $i_1, i_2, \dots, i_k$ , but not  $i_k, \dots, i_2, i_1$ . Then

$$f_e(n, k) = \frac{1}{2}(n^k + n^{\lceil \frac{k}{2} \rceil}). \quad (1)$$

*Proof.* By induction. For  $k = 1$ , there are  $n^k = n$  tuples and no reversals. For  $k = 2$ , the tuples correspond to the lower triangular part, including the diagonal, of an  $n \times n$  matrix,  $f_e(n, 2) = \sum_{i=1}^n i = \frac{n(n+1)}{2}$ . For  $k \rightarrow k + 1$ , consider the  $k$ -tuple  $s = (i, i', \dots, j', j)$  during lexicographic enumeration.

Case 1:  $i < j$ .  $\text{reverse}(s)$  has not been enumerated yet, and  $s$  is counted. Case 2:  $i > j$ .  $\text{reverse}(s)$  has been enumerated already, and  $s$  is not counted. Case 3:  $i = j$ . Recursively depends on  $(i', \dots, j')$ , with  $f_e(n, k - 2)$  possibilities to count. Together, cases 1 and 3 yield

$$f_e(n, k) = (n - 1)n^{k-2} + (n - 2)n^{k-2} + \dots + 1n^{k-2} + nf_e(n, k - 2) = \frac{n(n - 1)}{2}n^{k-2} + nf_e(n, k - 2),$$

which equates to (1), where  $\lceil \frac{k}{2} \rceil = \lceil \frac{k-2}{2} \rceil + 1$  can be seen by distinguishing odd and even  $k$ . □

### Indexing functions

The (1-based) indexing functions  $h_e(i_1, \dots, i_k)$  map  $k$ -tuples over  $\{1, \dots, n\}$  to consecutive indices  $1, 2, \dots$ , considering invariants and constraints of  $g$  (here, reversals). The first four are

$$h'_e(i_1) = i_1, \quad (2)$$

$$h'_e(i_1, i_2) = (i_1 - 1)(2n - i_1)/2 + i_2, \quad \text{where } i_1 \leq i_2, \quad (3)$$

$$h'_e(i_1, i_2, i_3) = (i_1 - 1)(n(n + 1 - i_1/2) - i_2) + i_3 + (i_2 - 1)n, \quad \text{where } i_1 \leq i_3, \quad (4)$$

$$h'_e(i_1, i_2, i_3, i_4) = -((i_1 - 1)n + i_2 - 1)((i_1 - 1 - 2n)n + i_2 - 2)/2 + i_4 + (i_3 - 1)(n - i_1) - i_1 + \max(i_3 - i_2 + 1, 0), \quad \text{where } i_1 \leq i_4 \text{ and } i_2 \leq i_3 \text{ for } i_1 = i_4. \quad (5)$$

*Proof.* Consider generating all  $k$ -tuples in lexicographic order while respecting invariances by skipping reversals, or, equivalently, by retaining only cases for which

$$\begin{array}{ll} k = 1: & \text{no restrictions} & k = 3: & i_1 \leq i_3 \\ k = 2: & i_1 \leq i_2 & k = 4: & i_1 \leq i_4 \text{ and } i_2 \leq i_3 \text{ if } i_1 = i_4 \end{array} \quad \cdot$$

These constraints exclude the lexicographically later-ranked reversal of each sequence, and only these. One arrives at the indexing functions by counting blocks of enumerated tuples in increasing index order:

$$h'_2(i_1, i_2) = \sum_{i=1}^{i_1-1} (n - i + 1) + i_2 - i_1 + 1,$$

$$\begin{aligned}
h'_3(i_1, i_2, i_3) &= \sum_{i=1}^{i_1-1} (n-i+1)n + \sum_{j=1}^{i_2-1} (n-i_1+1) + i_3 - i_1 + 1, \\
h'_4(i_1, i_2, i_3, i_4) &= \sum_{i=1}^{i_1-1} \underbrace{\left( (n-i)n^2 + \sum_{j=1}^n (n-j+1) \right)}_{i_1=i_4} + \sum_{j=1}^{i_2-1} \underbrace{\left( (n-j+1) + (n-i_1)n \right)}_{i_1 < i_4} \\
&\quad + \sum_{k=1}^{i_3-1} \underbrace{\left( \delta_{k \geq i_2} + (n-i_1) \right)}_{i_1=i_4} + \underbrace{i_4 - i_1 - \delta_{i_2 > i_3}}_{i_1 < i_4} + 1.
\end{aligned}$$

Applying sum formulae and rearranging terms yields (2)–(5).  $\square$

## Enumeration of atom tuples

Enumeration of all interactions between  $k$  atoms in a system of  $n$  atoms corresponds to enumeration of all  $k$ -tuples over  $\{1, \dots, n\}$ . Many choices of  $g$  are invariant to reversal and require distinct atoms. For example, the inverse distance between an atom and itself is undefined, as are angles if two of the three participating atoms are identical. In the following, we exclude reversed tuples and repeated atom indices. Note that this is equivalent to enumerating all length- $k$  prefixes of permutations of  $\{1, \dots, n\}$  ( $k$ -permutations) up to reversals. For MBTR calculations, the order of enumeration does not matter.

### Number of $k$ -body interactions

Let  $f_a(n, k)$  denote the number of  $k$ -tuples over  $\{1, \dots, n\}$  without repetitions and reversals. Then

$$f_a(n, k) = \frac{1}{2} \binom{n}{k} k! = \frac{1}{2} \prod_{i=0}^{k-1} (n-i) \quad \text{for } k > 1. \quad (6)$$

For  $1 \leq k \leq 4$ , these are  $f_a(n, 1) = n$ ,  $f_a(n, 2) = n(n-1)/2$ ,  $f_a(n, 3) = (n^3 - 3n^2 + 2n)/2$ ,  $f_a(n, 4) = (n^4 - 6n^3 + 11n^2 - 6n)/2$ .

*Proof.* Consider the  $k$ -tuple  $s = (i, i', \dots, j', j)$  during lexicographic enumeration. If  $i < j$ ,  $\text{reverse}(s)$  has not been enumerated yet, and  $s$  is counted. If  $i > j$ ,  $\text{reverse}(s)$  has been enumerated already, and  $s$  is not counted. The remaining case  $i = j$  constitutes a repetition, and  $s$  is not counted. This yields

$$f_a(n, k) = \sum_{i=1}^n (n-i) \prod_{j=1}^{k-2} (n-j-1).$$

$\square$

## References

- [1] Grégoire Montavon, Matthias Rupp, Vivekanand Gobre, Alvaro Vazquez-Mayagoitia, Katja Hansen, Alexandre Tkatchenko, Klaus-Robert Müller, and O. Anatole von Lilienfeld. Machine learning of molecular electronic properties in chemical compound space. *New J. Phys.*, 15(9):095003, 2013.
- [2] Matthias Rupp, Alexandre Tkatchenko, Klaus-Robert Müller, and O. Anatole von Lilienfeld. Fast and accurate modeling of molecular atomization energies with machine learning. *Phys. Rev. Lett.*, 108(5):058301, 2012.
- [3] Bing Huang and O. Anatole von Lilienfeld. Communication: Understanding molecular representations in machine learning: the role of uniqueness and target similarity. *J. Chem. Phys.*, 145(16):161102, 2016.
- [4] Sandip De, Albert P. Bartók, Gábor Csányi, and Michele Ceriotti. Comparing molecules and solids across structural and alchemical space. *Phys. Chem. Chem. Phys.*, 18(20):13754–13769, 2016.
- [5] Stefan Chmiela, Alexandre Tkatchenko, Huziel E. Sauceda, Igor Poltavsky, Kristof Schütt, and Klaus-Robert Müller. Machine learning of accurate energy-conserving molecular force fields. *Sci. Adv.*, 3(5):e1603015, 2017.
- [6] Stefan Chmiela, Huziel E. Sauceda, Klaus-Robert Müller, and Alexandre Tkatchenko. Towards exact molecular dynamics simulations with machine-learned force fields. *Nat. Commun.*, 9:3887, 2018.